α-D-Glucose-1,6-Biphosphate Induces Dendritic Cell Homing to Enhance the Antitumor Effect of Neoantigen Vaccines

Rui Zhang, Lin Tang, Yusi Wang, Qing Li, and Li Yang

Neoantigen vaccines have achieved good therapeutic effects in animal experiments and early clinical trials on certain malignant tumors. However, their overall objective effectiveness in clinical trials still needs to be improved. Low-efficiency dendritic cell (DC) migration (<5%) to lymph nodes is one of the factors that limits vaccine effectiveness. For neoantigen vaccines, improving the homing efficiency of DCs is expected to further improve the immunotherapeutic effect. In this study, we used α-D-glucose-1,6-biphosphate (α-D-Glu), a metabolite that successfully enhanced C57BL/6J mouse bone marrow–derived DC homing induced by neoantigen peptide, mRNA, and DC vaccines during the administration process and improved the antitumor effects in the mouse C57BL/6J model with a neoantigen vaccine. We clarified that α-D-Glu activated MAPK8IP1 by inhibiting the expression of microRNA-10a-5p, thereby activating the MAPK signaling pathway to promote DC homing. Excitingly, the efficiency of α-D-Glu in promoting DC migration is not weaker than that of PGE_2, which is the gold standard used to promote DC migration in clinical trials of DC vaccines. Thus, this study lays the foundation for further enhancing the objective clinical response rate of neoantigen vaccines and overcoming the limitation of an insufficient clinical response rate for neoantigen vaccines caused by low DC homing efficiency. ***The Journal of Immunology*****, 2023, 211: 1–12.**

In recent years, the development of sequencing technologies and bioinformatics has advanced research on individualized vaccines based on tumor-specific mutations (neoantigens), and personalized tumor-specific therapeutic vaccines based on neoantigens have been found to be immunogenic, safe, feasible therapeutic agents in patients with melanoma or glioblastoma (1–4) and to show promise for use in combination with other therapies, such as immune checkpoint inhibitor therapies (5, 6). Currently, there are three main types of neoantigen-based vaccine: neoantigen peptide vaccines, mRNA vaccines, and dendritic cell (DC) vaccines loaded with neoantigens.

After the administration of neoantigen vaccines, the immune response cascade begins with the homing of Ag-loaded DCs to the lymph nodes (LNs) and subsequent presentation of Ags to T cells. Among the various functional characteristics of DCs, the endogenous migratory activity of DCs, specifically the ability of DCs to migrate from the injection site to the draining LNs (dLNs) after injection of an in vitro–prepared DC vaccine, is key. This process controls the interaction between DCs and adaptive immune cells and activates adaptive immunity (7). However, a previous study found that the efficiency of DC migration from the injection site to the LNs induced by DC vaccination is very low, typically <5% (7). The low migration rate of DCs may be one of the major factors limiting the efficiency of DC vaccines. Importantly, the efficacy of DC vaccines has been shown to be strongly correlated with the efficiency of DC migration to the dLNs (8). Studies have shown that enhanced migration of DCs to the dLNs can induce stronger antitumor immune responses and improve patient survival (8). The more DCs that migrate to the dLNs, the more beneficial DC vaccines are (8). Therefore, we believe that improving the efficiency of DC migration to the dLNs will help further improve the antitumor effects of personalized neoantigen-based immunotherapies.

In our previous study, we identified several metabolites that control DC migration by metabolomic sequencing, namely, calcitriol, taurochenodeoxycholic acid (Tauro; MCE), 16(R)-HETE (GLPbio), acetylcholine (MCE), and α-D-glucose-1,6-biphosphate (α-D-Glu; GLPbio) (9). In this study, we proposed to select metabolites with optimal effects on DC migration, elucidate their mechanisms of DC migration control by transcriptomic and microRNA (miRNA) sequencing, and then try to combine the identified metabolites with classic neoantigen peptide vaccines, mRNA vaccines, and Ag-loaded DC vaccines to evaluate whether they can enhance the antitumor effects of the vaccines by promoting DC homing. The objective of these studies was to characterize the impacts of metabolites on DC function and migration in the context of neoantigen-based vaccines. In this study, we successfully enhanced DC homing induced by neoantigenic peptide, mRNA, and DC vaccines using α-D-Glu to improve the antitumor effect of the vaccine. We elucidated that α-D-Glu activates MAPK8IP1 by suppressing the expression of microRNA-10a-5p, which in turn activates the MAPK signaling pathway to promote DC homing. Excitingly, the efficiency of α-D-Glu in promoting DC migration was equal in human and murine DCs and was not weaker than that of PGE_2, the gold standard for promoting DC migration in clinical trials of DC vaccines (10, 11). Therefore, this study provides an option to improve the objective clinical response

Department of Biotherapy, Cancer Center and State Key Laboratory of Biotherapy, West China Hospital, Sichuan University, Chengdu, China

ORCIDs: 0000-0002-5508-8586 (R.Z.); 0000-0002-7880-2113 (L.Y.).

Received for publication September 15, 2022. Accepted for publication January 2, 2023.

This work was supported by the National Natural Science Foundation of China (Grants 32100748 and 82073366); the National Natural Science Foundation of Sichuan Province (Grant 2022NSFSC1642); the Post-Doctor Research Project, Sichuan University (Grant 2021SCU12028); and the Post-Doctor Research Project, West China Hospital, Sichuan University (Grant 2020HXBH173).

L.Y. and R.Z. designed the study. R.Z. is responsible for all experiments and articles. L.T., Y.W., and Q.L. helped R.Z. to perform the tumor model, the in vitro experiment, and the data analysis. All authors read and approved the final manuscript.

Address correspondence and reprint requests to Prof. Li Yang, Department of Biotherapy, Cancer Center and State Key Laboratory of Biotherapy, West China Hospital, Sichuan University, Chengdu 610041, China. E-mail address: yl.tracy73@gmail.com

The online version of this article contains supplemental material.

Abbreviations used in this article: BMDC, bone marrow–derived dendritic cell; DC, dendritic cell; α-D-Glu, α-D-glucose-1,6-biphosphate; dLN, draining lymph node; DPBS, Dulbecco's PBS; HOCl, hypochlorous acid; LN, lymph node; MoDC, monocyte derived dendritic cell; poly(I:C), polyinosinic-polycytidylic acid; PS, penicillin; Tauro, taurochenodeoxycholic acid; TCL, tumor cell lysate; Treg, regulatory T.

rate of neoantigenic vaccines and to improve their clinical response rate as a result of low DC homing efficiency.

Materials and Methods

Cells and animals

RPMI 1640 medium containing 100 U/ml streptomycin and penicillin (PS) and 10% FBS was used to culture bone marrow–derived DCs (BMDCs), EG7-OVA cells, and CT26 cells (American Type Culture Collection, Manassas, VA). All cells were cultured in a cell incubator containing 5% CO_2 at 37°C. RPMI 1640 medium, DMEM, FBS, and PS were all purchased from Thermo Fisher Scientific. Female 6- to 8-wk-old C57BL/6J mice were purchased from HFK Bioscience (Beijing, China). All animal procedures were approved and controlled by the Institutional Animal Care and Treatment Committee of Sichuan University and conducted according to the Animal Care and Use Guidelines of Sichuan University.

BMDCs were obtained from 4- to 6-wk-old C57BL/6J female mice according to a previously reported protocol (12). In brief, after treating bone marrow cells with RBC lysis buffer, fresh RPMI 1640 complete medium containing 20 ng/ml GM-CSF (PrimeGene Biotechnology, Shanghai, China) was added to 3×10^6 mouse bone marrow cells. On day 8, BMDCs were collected for further use.

Monocyte derived dendritic cells (MoDCs) were generated from human PBMCs according to a previous report (13). In brief, plasma was separated from whole blood by centrifugation, and the WBCs were separated by human lymphocyte separation medium. Then, the cells were washed, and CSTTM AIM VTM medium containing 5% autologous serum was added. On days 0, 3, and 5, fresh culture medium supplemented with 1000 U/ml GM-CSF (Primegene Biotechnology), 500 U/ml recombinant human IL-4 (Primegene Biotechnology), and 5% autologous serum was added to the cells. RPMI 1640 medium, FBS, and PS were all purchased from Thermo Fisher Scientific (Waltham, MA).

CCK-8 assay

In 96-well plates, EG7-OVA (1×10^4) cells, CT26 (1×10^4) cells, and BMDCs (5×10^4) were plated. After incubation for 24 h at 37°C, cells were treated with different concentrations of α-D-Glu for another 24 h. Subsequently, 10 μl of CCK-8 solution was added and incubated at 37°C for 1 h. Then, a SpectraMax M5 Microtiter Plate Luminometer (Molecular Devices, Sunnyvale, CA) was used to detect the absorbance at 450 nm. The absorbance of untreated cells was considered to be 100%.

Cell migration assay

In in vitro migration experiments, DCs (3×10^5 cells/ml) treated with calcitriol (10 nM), Tauro (50 μM), 16(R)-HETE (0.5 μM), acetylcholine (1 μM), α-D-Glu (15 μM), PGE_2 (250 ng/ml; PeproTech), and TNF-α (10 ng/ml; PrimeGene Biotechnology) + IL-1β (10 ng/ml; PrimeGene Biotechnology) + IFN-γ (1000 U/ml; PrimeGene Biotechnology) + R848 (1 μg/ml; InvivoGen) + polyinosinic-polycytidylic acid [poly(I:C); 20 ng/ml; InvivoGen] + PGE_2 (250 ng/ml)/α-D-Glu (15 μM)/PGE_2 (250 ng/ml) + α-D-Glu (15 μM) for 24 h were collected and transferred to a transwell plate (NEST Biotechnology Co., Ltd.). The upper chamber contained 1×10^5 cells in 100 μl of RPMI 1640 medium. The lower chamber contained 500 μl of RPMI 1640 medium with 10% FBS (VivaCell, Shanghai, China) + CCL19 (250 ng/ml) + CCL21 (250 ng/ml; Sino Biological). The cells in the upper chamber and lower chamber were counted after 24 h (Countstar). Migration efficiency = total number of lower chamber cells/(total number of lower chamber cells + total number of upper chamber cells).

ERK1/2 activity was inhibited by treating cells with KO-947 (10 nM; TargetMol) for 1 h before the migration assay (14). To verify whether high expression of miR-10a-5p can inhibit α-D-Glu–induced DC migration, we used Lipo3000 (0.48 μg; Invitrogen, Carlsbad, CA) to transfect DCs (5×10^5) with miR-10a-5p mimics (miR-10a-5p, 0.24 μg) or a miR-10a-5p inhibitor (in 10a-5p, 0.24 μg) for 4 h and then added α-D-Glu (15 μM) for another 20 h before performing the migration experiments. All tests were repeated three times. In in vivo migration experiments, DCs (3×10^5/ml) treated with PBS, α-D-Glu (15 μM), LPS (1 μg/ml) + CpG (10 μg/ml) + IFN-γ (50 ng/ml) + $OVA_{257–264}$ (10 μg/ml; Shanghai Apeptide), or α-D-Glu (15 μM) + LPS (1 μg/ml) + CpG (10 μg/ml) + IFN-γ (50 ng/ml) + $OVA_{257–264}$ (10 μg/ml) for 24 h were collected and labeled with CFSE (Beyotime Biotechnology, Shanghai, China) according to the instructions of the kit. Labeled DCs were then injected into the hind foot pads of mice (1×10^6/50 μl). After 24 h, the dLNs (inguinal LNs) were harvested, and cells in the dLNs were collected with a needle. Finally, the proportion of carboxyfluorescein succinimidyl ester–positive cells in the dLNs was detected by flow cytometry.

Flow cytometry assay

To detect DC homing, DC Ag presentation efficiency, and DC maturation in vivo, we s.c. injected mice with PBS, poly(I:C) (50 μg/each) + $OVA_{257–264}$ (10 μg/each), α-D-Glu (150 μM/each) + poly(I:C) (50 μg/each) + $OVA_{257–264}$ (10 μg/each), DOTAP (20 μg/each) (AVT (Shanghai) Pharmaceutical Tech Co., Ltd.) + OVA mRNA (10 μg/each; Tebu-bio), or α-D-Glu (150 μM/each) + DOTAP (20 μg/each) + OVA mRNA (10 μg/each), and then the LNs were removed 24 h later and punctured using a needle to fully release the cells. Finally, DC homing, Ag presentation efficiency, and maturation were detected by staining with an anti-mouse CD11c-allophycocyanin Ab, or an anti-mouse CD11c-allophycocyanin Ab and the 25-D1.16-PE mAb, or anti-mouse CD11c-allophycocyanin Ab, anti-mouse CD80-PerCP Ab, and anti-mouse CD86-FITC Ab for 40 min followed by flow cytometry analysis. All tests were repeated three times. The inguinal LNs at the injection site were defined as the proximal LNs, and those on the other side were the distal LNs.

To detect the efficiencies of Ag uptake, Ag presentation by BMDCs, and BMDC maturation in vitro, we incubated BMDCs (5×10^5/ml) with PBS, calcitriol (10 nM), Tauro (50 μM), 16(R)-HETE (0.5 μM), acetylcholine (1 μM), or α-D-Glu (15 μM), with or without (1) poly(I:C) (50 μg/ml) + FITC-$OVA_{257–264}$/$OVA_{257–264}$ (10 μg/ml) and (2) LPS (1 μg/ml; Beyotime Biotechnology) + CpG (CpG 1826 oligonucleotide, 10 μg/ml; Invitrogen) + IFN-γ (50 ng/ml; PrimeGene Biotechnology) + FITC-$OVA_{257–264}$/$OVA_{257–264}$ (10 μg/ml) for 24 h. Then, the Ag uptake, Ag presentation efficiency, and maturation of DCs were detected by staining with an anti-mouse CD11c-allophycocyanin Ab, an anti-mouse CD11c-allophycocyanin Ab and the 25-D1.16-PE mAb, or an anti-mouse CD11c-allophycocyanin Ab, an anti-mouse CD80-PerCP Ab, and an anti-mouse CD86-FITC for 40 min followed by flow cytometry analysis. All tests were repeated three times.

To detect the efficiencies of MoDC maturation in vitro, we incubated MoDCs (5×10^5/ml) with PBS, α-D-Glu (15 μM), PGE_2 (250 ng/ml), TNF-α (10 ng/ml) + IL-1β (10 ng/ml) + IFN-γ (1000 U/ml) + R848 (1 μg/ml) + poly(I:C) (20 ng/ml) + PGE_2 (250 ng/ml)/α-D-Glu (15 μM)/PGE_2 (250 ng/ml) + α-D-Glu (15 μM) with or without $OVA_{257–264}$ (10 μg/ml) for 24 h. Then, the Ag presentation efficiency and maturation of DCs were detected by staining with an anti-human CD11c-FITC Ab and the 25-D1.16-PE mAb or an anti-human CD11c-PE Ab, an anti-human CD86-FITC Ab, and an anti-human CD83-allophycocyanin Ab for 40 min followed by flow cytometry analysis. All tests were repeated three times.

To detect inhibition of DC homing in vivo by pretreatment of KO-947, we pregavaged mice with KO-947 (300 mg/kg) for 24 h (14), then s.c. injected them with poly(I:C) (50 μg/each) + $OVA_{257–264}$ (10 μg/each), α-D-Glu (150 μM/each) + poly(I:C) (50 μg/each) + $OVA_{257–264}$ (10 μg/each), DOTAP (20 μg/each) + OVA mRNA (10 μg/each), or α-D-Glu (150 μM/each) + DOTAP (20 μg/each) + OVA mRNA (10 μg/each); next, the LNs were removed 24 h later and punctured using a needle to fully release the cells. Finally, DC homing was detected by staining with an anti-mouse CD11c-PE Ab for 40 min followed by flow cytometry analysis. All tests were repeated three times.

To detect the proportion of T cells in the spleen and LNs after vaccine injection, we harvested cells from the spleen and LNs at 24 h after injection of (1) PBS, (2) poly(I:C) (50 μg/each) + $OVA_{257–264}$ (10 μg/each), (3) α-D-Glu (150 μM/each) + poly(I:C) (50 μg/each) + $OVA_{257–264}$ (10 μg/each), (4) DOTAP (20 μg/each) + OVA mRNA (10 μg/each), (5) α-D-Glu (150 μM/each) + DOTAP (20 μg/each) + OVA mRNA (10 μg/each), (6) DCs (1×10^6/ml) loaded with $OVA_{257–264}$ (10 μg/ml) + LPS (1 μg/ml) + CpG (10 μg/ml) + IFN-γ (50 ng/ml), or (7) α-D-Glu (15 μM) + DCs (1×10^6/ml) loaded with $OVA_{257–264}$ (10 μg/ml) + LPS (1 μg/ml) + CpG (10 μg/ml) + IFN-γ (50 ng/ml). Single-cell suspensions were obtained from the spleen after mechanical dissociation with a syringe, sieve filtration, and RBC lysis and from the LNs after collection with a needle tip and filtration. Staining with an anti-mouse CD3-allophycocyanin Ab, anti-mouse CD8-PerCP Ab, anti-mouse CD4-FITC Ab, and anti-mouse CD25-allophycocyanin-Cy7 Ab was carried out at 4°C. Staining with an anti-mouse Foxp3-PE Ab was carried out after cells were fixed and permeabilized following surface staining. The staining time was 40 min for each round of staining. After staining, excess Abs were removed by washing with PBS. Finally, the percentages of $CD3^+CD8^+$ T cells, $CD3^+CD4^+$ T cells, and regulatory T (Treg; $CD3^+CD4^+CD25^+Foxp3^+$) cells were measured by flow cytometry.

Real-time quantitative RT-PCR

For the in vitro study, RNA was extracted from mouse bone marrow–derived DCs (BMDCs; with purity >90%), which were treated with PBS or α-D-Glu (15 μM) for 24 h, with RNA isolator total RNA extraction reagent (Vazyme Biotech). For the in vivo study, RNA was extracted from DCs isolated from mouse LNs treated with PBS or α-D-Glu (150 μM) for 24 h. After reverse transcription of the extracted RNA with HiScript II Q RT

SuperMix for quantitative PCR or the miRNA 1st Strand cDNA Synthesis Kit (Vazyme Biotech), the produced cDNA was used for mouse chemokine and chemokine receptor expression analysis or miRNA expression analysis according to the manufacturer's instructions. miRNA expression levels were normalized to the U6 level in each sample.

Cytokine detection

The supernatants of BMDCs (3×10^5 cells/ml) treated with PBS, α-D-Glu (15 μM), KO-947 (10 nM, 1 h before α-D-Glu addition) + α-D-Glu (15 μM), Lipo3000 (0.48 μg) + miRNA negative control (0.24 μg), Lipo3000 (0.48 μg) + miR-10a-5p mimics (miR10a-5p, 0.24 μg), Lipo3000 (0.48 μg) + inhibitor negative control (0.24 μg), or Lipo3000 (0.48 μg) + miR-10a-5p inhibitor (in10a-5p, 0.24 μg) were collected, and the levels of CCL21 were detected with an ELISA kit (Beijing Solarbio Science & Technology Co., Ltd.) according to the vendor's instructions. All tests were repeated three times.

The supernatants of MoDCs (3×10^5 cells/ml) treated with PBS, α-D-Glu (15 μM), PGE_2 (250 ng/ml), TNF-α (10 ng/ml) + IL-1β (10 ng/ml) + IFN-γ (1000 U/ml) + R848 (1 μg/ml) + poly(I:C) (20 ng/ml) + PGE_2 (250 ng/ml)/α-D-Glu (15 μM)/PGE_2 (250 ng/ml) + α-D-Glu (15 μM) were collected, and the levels of IL-12p70 and IL-10 were detected with an ELISA kit (Shanghai ZCIBIO Technology Co., Ltd.) according to the vendor's instructions. All tests were repeated three times.

Transcriptomic sequencing

BMDCs (purity ≥ 90%, 1×10^7) were treated with PBS or α-D-Glu (15 μM) for 4 h ($n = 3$), and then the residual drug was removed by washing. The cells were lysed with TRIzol (Invitrogen). Finally, the samples were sent to Novogene (Beijing, China) for transcriptomic sequencing using an Illumina NovaSeq 6000 system. Once the company completed quality control, sequencing, and data analysis, Novomagic was used for subsequent data processing.

miRNA sequencing

BMDCs (purity ≥ 90%, 1×10^7) were treated with PBS or α-D-Glu (15 μM) for 24 h ($n = 3$), the residual drug was removed by washing, and the cells were lysed with TRIzol. Then, the samples were sent to Novogene (Beijing, China) for miRNA sequencing using the Illumina SE50 system. Once the company completed quality control, sequencing, and data analysis, Novomagic was used for subsequent data processing.

Western blot analysis

Total protein was extracted from DCs treated with PBS or α-D-Glu (15 μM) for 30 min or 4 h. Total protein was extracted from DCs transfected with Lipo3000/miRNA negative control, Lipo3000/mi10a-5p (5′-UACCCUGUAGAUCCGAAUUUGUG-3′; GenePharma, Shanghai, China), Lipo3000/inhibitor negative control, or Lipo3000/in10a-5p for 24 h. The protein lysates were subjected to $NaDodSO_4$ PAGE and transferred to membranes. Then, the membranes were probed with Abs against GAPDH, MAPK8IP1, ERK1/2, and p-ERK1/2 HUABIO and incubated with an HRP-conjugated secondary Ab (Abcam). Finally, a chemiluminescence system (Millipore, MA) was used to visualize and photograph the target protein bands.

Preparation of hypochlorous acid–oxidized tumor cell lysates

We followed the protocol from a previous report to prepare hypochlorous acid (HOCl)-oxidized CT26 lysate (15). In brief, NaOCl reagent (Sigma-Aldrich) was diluted with Dulbecco's PBS (DPBS; Cellgro) and immediately added to the tumor cells to prepare a 0.7 μM HOCl solution. The final cell density was 1×10^6 cells/ml in DPBS. The tumor cell suspensions were incubated at 37°C for 1 h with gentle agitation every 30 min to induce oxidation-dependent tumor cell death. At the end of the 1-h treatment, the tumor cells were harvested, washed twice with DPBS (three times the volume of DPBS was added to each volume of HOCl solution to ensure complete removal of HOCl), and subjected to seven freeze–thaw cycles. For this, the tumor cell lysates (TCLs) were frozen in liquid nitrogen for ≥5min and thawed completely at room temperature seven times to completely rupture the tumor cells.

In vivo immunization and cancer immunotherapy studies

For verification of whether α-D-Glu has direct antitumor effects in vivo, mice were divided into four groups (PBS, α-D-Glu [50 μM/each], α-D-Glu [150 μM/each], and α-D-Glu [450 μM/each]), with five mice in each group. On day 0, EG7-OVA tumor cells (1×10^6/100 μl/mouse) were s.c. injected into the mice. On days 1, 4, 8, 11, and 15, α-D-Glu was s.c. injected into the mice in each group. Tumor volumes were recorded every 3 d.

To verify whether α-D-Glu can enhance the antitumor effect of a poly(I:C)+$OVA_{257–264}$ vaccine, we divided mice into three groups [PBS, poly(I:C) (50 μg/each) + $OVA_{257–264}$ (10 μg/each), and α-D-Glu (150 μM/each) + poly(I:C) (50 μg/each) + $OVA_{257–264}$ (10 μg/each)], with six mice in each group. On day 0, EG7-OVA tumor cells (1×10^6/100 μl/mouse) were s.c. injected into the mice. On days 1, 4, 8, 11, and 15, poly(I:C)+$OVA_{257–264}$ or α-D-Glu+poly(I:C)+$OVA_{257–264}$ was s.c. injected into the mice in each group. The mice were sacrificed on day 18, and the tumors were weighed and photographed. Body weight and tumor volume were recorded every 2 d.

To verify whether α-D-Glu can enhance the antitumor effect of a DOTAP+OVA mRNA vaccine, we divided mice into three groups (PBS, DOTAP [20 μg/each] + OVA mRNA [10 μg/each], and α-D-Glu [150 μM/each] + DOTAP [20 μg/each] + OVA mRNA [10 μg/each]), with each group containing five mice. On day 0, EG7-OVA tumor cells (1×10^6/100 μl/mouse) were s.c. injected into the mice. On days 1, 4, 8, 11, and 15, DOTAP+OVA mRNA or α-D-Glu+DOTAP+OVA mRNA was s.c. injected into the mice in each group. The mice were sacrificed on day 18, and the tumors were weighed and photographed. Body weight and tumor volume were recorded every 2 d.

To verify whether α-D-Glu can enhance the antitumor effect of DCs loaded with an $OVA_{257–264}$ vaccine, we divided mice into three groups (PBS, DCs [1×10^6/ml] loaded with $OVA_{257–264}$ [10 μg/ml] + LPS [1 μg/ml] + CpG [10 μg/ml] + IFN-γ [50 ng/ml], and α-D-Glu [15 μM] + DCs [1×10^6/ml] loaded with $OVA_{257–264}$ [10 μg/ml] + LPS [1 μg/ml] + CpG [10 μg/ml] + IFN-γ [50 ng/ml]), with each group containing six mice. On day 0, EG7-OVA tumor cells (1×10^6/100 μl/mouse) were s.c. injected into the mice. On days 1, 4, 8, 11, and 15, DCs given the earlier treatments were s.c. injected into the mice in each group. The mice were sacrificed on day 18, and the tumors were weighed and photographed. Body weight and tumor volume were recorded every 2 d.

To verify whether α-D-Glu can enhance the antitumor effect of DCs loaded with an CT26-TCL vaccine, we divided mice into four groups (PBS, DCs [1×10^6/ml] loaded with CT26-TCL [3×10^5 cells/ml] + LPS [1 μg/ml] + CpG [10 μg/ml] + IFN-γ [50 ng/ml], α-D-Glu [15 μM] + DCs [1×10^6/ml] loaded with CT26-TCL [3×10^5 cells/ml] + LPS [1 μg/ml] + CpG [10 μg/ml] + IFN-γ [50 ng/ml], and PGE_2 [250 ng/ml] + DCs [1×10^6/ml] loaded with CT26-TCL [3×10^5 cells/ml] + LPS [1 μg/ml] + CpG [10 μg/ml] + IFN-γ [50 ng/ml]), with each group containing six mice. On day 0, CT26 tumor cells (1×10^6/100 μl/mouse) were s.c. injected into the mice. On days 1, 4, 8, 11, and 15, DCs (2×10^6/100 μl/mouse) given the earlier treatments were s.c. injected into the mice in each group. The mice were sacrificed on day 18, and the tumors were photographed. Tumor volumes were recorded every 3 d.

ELISPOT assay

For the ELISPOT assay, all mice were sacrificed on day 18, and spleen lymphocytes were harvested for experiments. The ELISPOT assay was performed according to the manufacturer's instructions. In brief, 2×10^5 mouse spleen lymphocytes were seeded in a 96-well microtiter plate precoated with an anti–IFN-γ Ab. Next, 10 μg/ml wild-type peptides or mutant peptides was added, and the plate was incubated at 37°C. After 48 h, the culture medium was aspirated from the wells, and precooled ddH_2O was added at 4°C for 10 min to lyse the cells. The plate was then washed five times with wash buffer. Next, a diluted biotinylated secondary Ab was added to each well, followed by incubation for 1 h at 37°C. For enzyme-linked avidin incubation, a diluted avidin enzyme working solution was added to each well and incubated at 37°C for 1 h. A prepared aminoethyl carbazole solution was then added, and the color reaction was allowed to occur at 37°C in the dark for ~15 min. Finally, the plates were photographed and read using a BioReader 4000 (Byosys, Karben, Germany).

Histological analysis

After the mice in each group were sacrificed, the main organs were harvested, fixed immediately using 4% paraformaldehyde, and embedded in paraffin. Embedded tissue sections were dewaxed and rehydrated before staining with Mayer's H&E according to the vendor's instructions (Solarbio, China).

Statistical analysis

All data were evaluated and plotted using GraphPad Prism 9.0. Student's *t* test and one-way or two-way ANOVA were used to analyze differences in data. A p value <0.05 was considered statistically significant.

Data availability

The datasets generated and/or analyzed during this study are available from the corresponding author on reasonable request.

Results

α-D-Glu can enhance the antitumor effect of neoantigen (peptide or mRNA) vaccines and DC vaccines loaded with neoantigen

To verify whether α-D-Glu can enhance the antitumor effects of the poly(I:C)+$OVA_{257–264}$ vaccine (neoantigen peptide vaccine), the DOTAP+OVA mRNA vaccine (mRNA vaccine), or DC vaccines loaded with $OVA_{257–264}$, we performed experiments according to the processes shown in Fig. 1A and 1B. The results showed that α-D-Glu alone is not toxic to tumor cells and DCs and has no direct tumor-killing effect in vivo (Supplemental Fig. 1A, 1B). The antitumor effect increased significantly after α-D-Glu was added to vaccine components, and this effect was reflected by significant decreases in tumor growth in all of the vaccine combinations with α-D-Glu groups versus the other control groups (Fig. 1C–H, Supplemental Fig. 1C). Then, we evaluated the safety of combination therapy with each of the three vaccines and α-D-Glu by recording mouse weights during vaccine treatment and by H&E staining of the main organs of mice after vaccine treatment. The results showed that no obvious toxicities or side effects were found in the main organs after vaccine treatment (Supplemental Fig. 1D–G), which preliminarily indicated that combination therapy with each of the three vaccines and α-D-Glu was safe.

α-D-Glu promoted DC migration in vivo *and* in vitro *without affecting the uptake or presentation of Ags by DCs or the efficiency of DC maturation*

To verify the effects of specific metabolites on DC function, we performed in vitro experiments to evaluate the effects of metabolite treatment on DC uptake of an Ag, presentation of the Ag, maturation, and migration efficiency. The results showed that acetylcholine, 16(R)-HETE, Tauro, and α-D-Glu were able to promote DC migration (Supplemental Fig. 2A). These metabolites essentially did not affect the efficiency of Ag uptake by DCs or the proportion of $CD11c^+$ cells (Supplemental Fig. 2B, 3A, 3D). The results also showed that acetylcholine, calcitriol, Tauro, and 16(R)-HETE essentially reduced the efficiency of DC presentation of Ags (Supplemental Fig. 2C, 3E). In terms of DC maturation, calcitriol and Tauro inhibited DC maturation (Supplemental Fig. 2D, 3F). Overall, we found that α-D-Glu was the most effective metabolite for promoting DC migration, and that it did not affect the Ag uptake or presentation efficiency of DCs or DC maturation efficiency. Thus, we chose α-D-Glu as the research object in a follow-up experiment.

We tested the effects of α-D-Glu combined with poly(I:C)+$OVA_{257–264}$, DOTAP+OVA mRNA, or DCs loaded with $OVA_{257–264}$

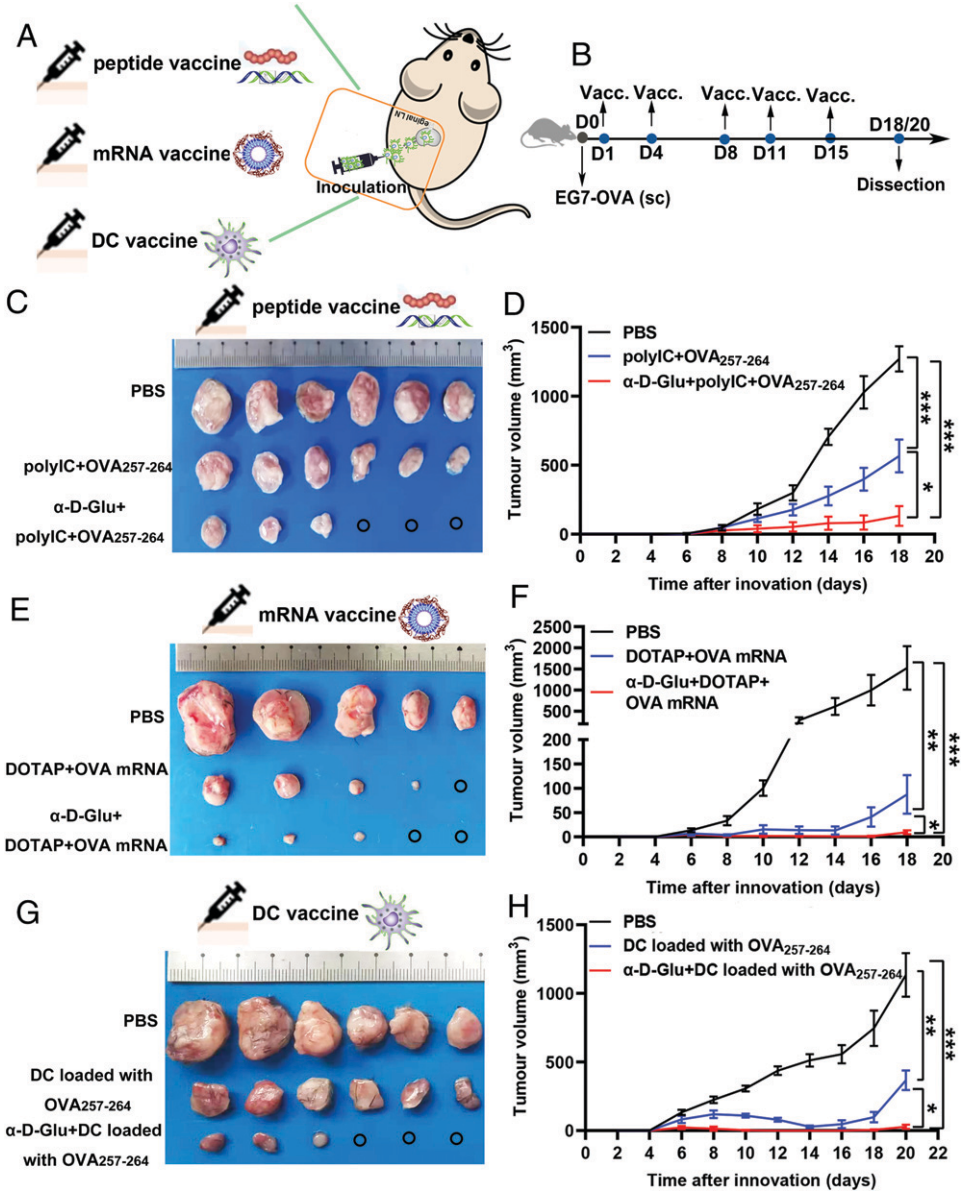

FIGURE 1. α-D-Glu enhanced the antitumor effect of the poly(I:C)+$OVA_{257–264}$ vaccine, DOTAP+OVA mRNA vaccine, and DC vaccine loaded with LPS+CPG+IFN-γ+$OVA_{257–264}$. (**A** and **B**) Diagram of the vaccine workflow. (**C**) Representative results for mouse tumors of the poly(I:C)+$OVA_{257–264}$ vaccine groups ($n = 6$). (**D**) Mean tumor volume of the poly(I:C)+$OVA_{257–264}$ vaccine groups ($n = 6$). (**E**) Representative results for mouse tumors of the mRNA vaccine groups ($n = 5$). (**F**) Mean tumor volume of the mRNA vaccine groups ($n = 5$). (**G**) Representative results for mouse tumors of the DC vaccine groups ($n = 6$). (**H**) Mean tumor volume of the DC vaccine groups ($n = 6$). Significance was calculated using one-way ANOVA with multiple comparisons tests. $^*p < 0.05$, $^{**}p < 0.01$, $^{***}p < 0.001$.

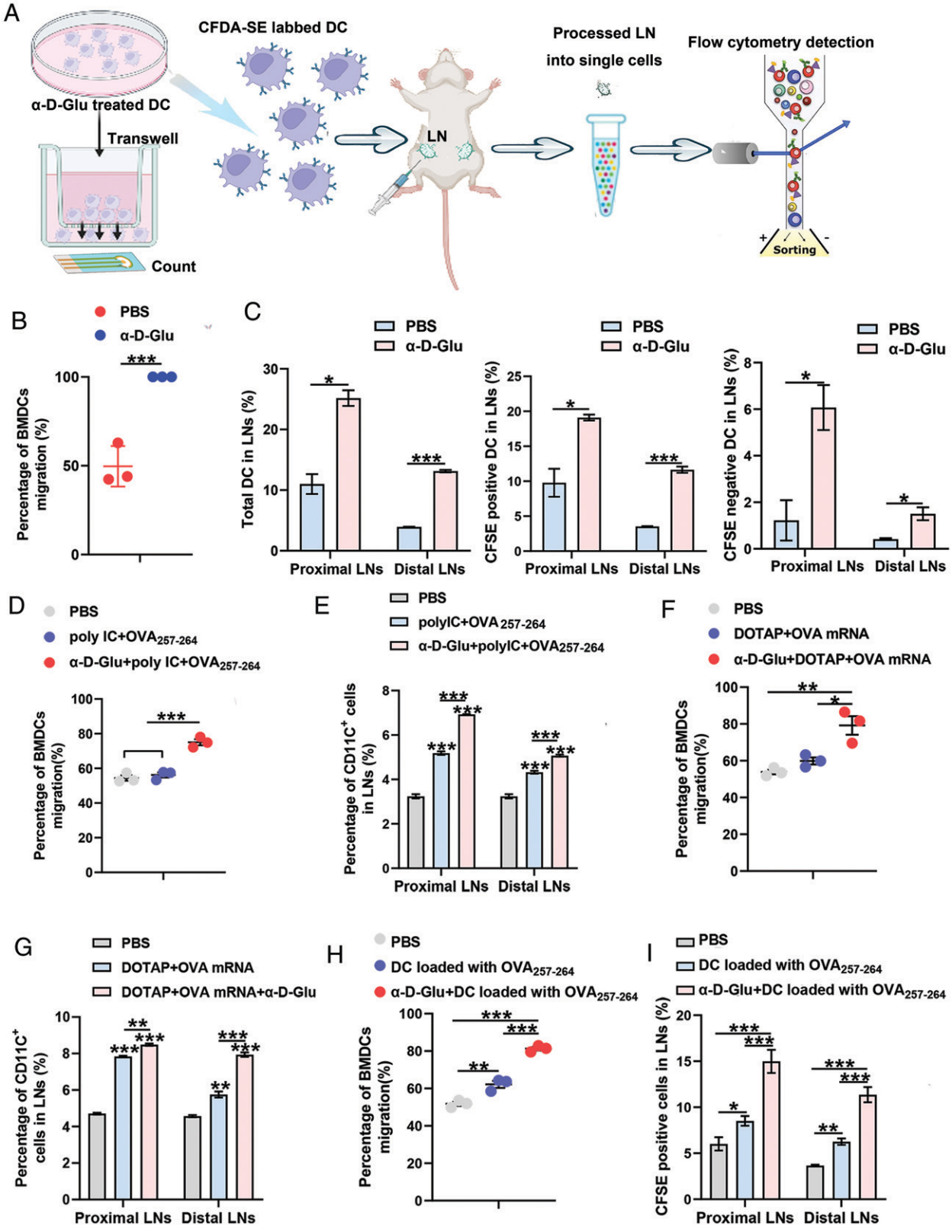

FIGURE 2. α-D-Glu enhanced the antitumor effect of the neoantigen vaccine by inducing DC homing. (**A**) Schematic diagram of the experimental procedure. (**B**) Detecting the effects of α-D-Glu on DC migration efficiency in vitro. (**C**) Detecting the effects of α-D-Glu on the in vivo migration of DCs. (**D**) Detecting the effects of α-D-Glu combined with poly(I:C)+$OVA_{257–264}$ on DC migration efficiency in vitro. (**E**) Detecting the effects of α-D-Glu+poly(I:C)+$OVA_{257–264}$ on the proportion of DCs in the LNs. (**F**) Detection of the effects of α-D-Glu combined with DOTAP+OVA mRNA on DC migration efficiency in vitro. (**G**) Detecting the effects of α-D-Glu+DOTAP+OVA mRNA on the proportion of DCs in the LNs. (**H**) Detecting the effects of α-D-Glu combined with DC vaccine loaded with LPS+CPG+IFN-γ+$OVA_{257–264}$ on DC migration efficiency in vitro. (**I**) Detecting the effects of α-D-Glu combined with DC vaccine loaded with LPS+CPG+IFN-γ+$OVA_{257–264}$ on the proportion of DCs in the LNs. All data are representative of results from three independent experiments ($n = 3$). Significance was calculated using one-way ANOVA with multiple comparisons tests. *$p < 0.05$, **$p < 0.01$, ***$p < 0.001$.

on DC migration in vitro, DC homing, Ag presentation, and maturation in the LNs. The results showed that α-D-Glu and its combination with the DC vaccine loaded with $OVA_{257–264}$, poly(I:C)+$OVA_{257–264}$, or DOTAP+OVA mRNA enhanced the in vitro migration efficacy and LN homing efficiency of DCs (Fig. 2A–I). α-D-Glu combined with poly(I:C)+$OVA_{257–264}$ or DOTAP+OVA mRNA did not enhance the poly(I:C)+$OVA_{257–264}$ or DOTAP+OVA mRNA-induced maturation of DCs or efficiency of DC presentation of Ags in the LNs (Supplemental Fig. 2E–G, 3B, 3C, 3G).

α-D-Glu combined with neoantigen vaccine administration changed the proportion of T cells in the spleen and LNs

PGE_2, which is commonly used clinically to promote DC migration, usually differentiates DCs into a subtype that promotes a type 2 or Treg response (7). Therefore, we tested the types of T cells induced in vivo by the three vaccines combined with α-D-Glu (Fig. 3A). The results showed that compared with the poly(I:C)+$OVA_{257–264}$ vaccine group, the α-D-Glu+poly(I:C)+$OVA_{257–264}$ vaccine group showed a significantly enhanced proportion of $CD3^+CD8^+$ T cells and $CD3^+CD4^+$ T cells in the LNs. There was no difference in $CD3^+CD8^+$ T cells in the spleen, but the proportion of $CD3^+CD4^+$ T cells was significantly enhanced, and the proportion of Tregs was significantly decreased (Fig. 3B, 3C). Compared with the DOTAP+OVA mRNA vaccine group, the α-D-Glu+DOTAP+OVA mRNA vaccine group showed a significantly enhanced proportion of $CD3^+CD8^+$ T cells and $CD3^+CD4^+$ T cells in the LNs and spleen (Fig. 3D, 3E). Compared with the DC vaccine group, the α-D-Glu+DC vaccine group showed a significantly enhanced proportion of $CD3^+CD8^+$ T cells and $CD3^+CD4^+$ T cells in the LNs and spleen, and the proportion of Tregs was significantly decreased (Fig. 3F, 3G). Finally, after the vaccine mice in Fig. 1 were sacrificed, we tested the Ag-specific lymphocyte response with an ELISPOT assay and found that the Ag-specific lymphocyte response of the experimental group with α-D-Glu added was significantly enhanced compared with that of the control group (Fig. 3H–J).

α-D-Glu induces DC migration by inhibiting miRNA-10a-5p and thereby activating the MAPK8IP1/ERK signaling pathway

Chemokines and their receptors have been reported to be critical for cell migration, so we examined the expression of various common chemokines and their receptors after α-D-Glu treatment (Fig. 4A). The results showed that the expression levels of CCL21, TNF-α, and XCR1 were obviously upregulated in treated versus untreated cells, and that the change in CCL21 was the most obvious (Fig. 4B–D). To further determine the specific mechanism by which α-D-Glu controls DC migration, we performed transcriptomic and miRNA sequencing of DCs after α-D-Glu treatment (Fig. 5A). The transcriptomic sequencing results showed that 306 genes were upregulated and 50 genes were downregulated in the treated group (Fig. 5B). The miRNA sequencing results showed that seven miRNAs were upregulated and three miRNAs were downregulated in the treated group (Fig. 5C). Then, through enrichment analysis of the signaling pathways containing the changed genes and enrichment analysis of the signaling pathways containing the target genes of all the changed miRNAs, we found that the regulation of the actin cytoskeleton signaling pathway and the MAPK signaling pathway was repeatedly enriched (Fig. 5D, 5E). Therefore, we speculated that α-D-Glu might promote DC migration by regulating the expression of miRNAs in the signaling pathways containing their target genes. We then performed protein interaction network analysis of all the altered genes in the two signaling pathways identified and found that the two signaling pathways jointly regulated ERK1/2 expression (Fig. 5F). We then verified that α-D-Glu activated p-ERK1/2 expression, and that α-D-Glu–induced cell migration was significantly inhibited after treatment with the ERK inhibitor KO-947 (Fig. 6B, 6C). Next, we verified the expression of all the changed miRNAs in the sequencing data and found that miR-486a-5p, miR100-5p, and miR-381-3p expression was upregulated, whereas miR-10a-5p and let-7j expression was downregulated (Fig. 5G, 6D). After analyzing the target genes of these miRNAs, we found that the target gene of upregulated miR-486a-5p in the MAPK pathway is PIK3R1, and the target gene of upregulated miR-100-5p in the MAPK pathway is rasgrp3, both of which are genes that positively regulate ERK and therefore are not consistent with the actual validation results. The target gene of upregulated miR-381-3p was not related to the MAPK signaling pathway, and its high expression is reported to inhibit cell migration (16), so this target gene is inconsistent with the actual verification results. The target gene of downregulated let-7j was not associated with the MAPK signaling pathway, and no correlation with cell migration has been reported. In contrast, the target gene of downregulated miR-10a-5p was MAPK8IP1 (17), which is upstream of ERK. This gene was highly expressed in the transcriptomic sequencing results and was most consistent with the actual results (Supplemental Fig. 4). Therefore, we speculated that α-D-Glu treatment may promote DC migration by inhibiting the expression of miR-10a-5p and upregulating MAPK8IP1, thus activating MAPK. We verified this finding, and the results showed that the expression of MAPK8IP1 was upregulated after DCs were treated with α-D-Glu (Fig. 6B). The expression of MAPK8IP1 and p-ERK1/2 was inhibited after transfection of miR-10a-5p into DCs, whereas this expression was activated after transfection of in10a-5p (Fig. 6E). Transfection of miR-10a-5p inhibited α-D-Glu–induced DC migration (Fig. 6F). In addition, we found that the activation of the MAPK signaling pathway was positively correlated with the secretion of CCL21 (18), and we verified that the ability of α-D-Glu–induced DCs to secrete CCL21 was inhibited by the ERK inhibitor (Fig. 6H). The secretion of CCL21 was significantly inhibited after transfection of miR-10a-5p, and this effect was significantly inhibited after transfection of in-10a-5p (Fig. 6H). In addition, α-D-Glu–induced DC migration was significantly inhibited after preinhibition of ERK in vivo (Fig. 6I, 6J). In addition, we isolated DCs from LNs of mice 24 h after α-D-Glu treatment and verified that among them, MAPK8IP1 and CCL21 expression was upregulated and miR10a-5p expression was downregulated (Fig. 6K–M). The earlier results showed that the DC migration induced by α-D-Glu was achieved by inhibiting the expression of miR-10a-5p, thereby activating MAPK8IP1 and p-ERK1/2 (Fig. 6A).

The effect of α-D-Glu in promoting MoDC migration is not weaker than that of PGE_2

In this study, we used MoDCs derived from lung cancer patients to further verify the function of α-D-Glu and compare it with PGE_2, which is commonly used in clinical trials to promote DC migration (Fig. 7A). The results showed that in the MoDCs from the three patients, α-D-Glu or PGE_2 alone could promote the migration of their MoDCs in vitro, and the effects of the two were equivalent. When they were used in combination with a formula that stimulates DC maturation [TNF-α+IL-1β+IFN-γ+poly(I:C)], they could also promote DC migration with equivalent effects (Fig. 7B). In addition, we also compared whether the combination of the two and MoDC maturation formula could inhibit DC maturation and cytokine secretion. The results showed that the combined formula had no effect on DC maturation and no effect on DC secretion of IL-10, but it improved the ability of DCs to secrete IL-12p70 (Fig. 7C–E).

Discussion

In recent years, scientists around the world have reported major breakthroughs in the field of immunotherapy, and major pharmaceutical

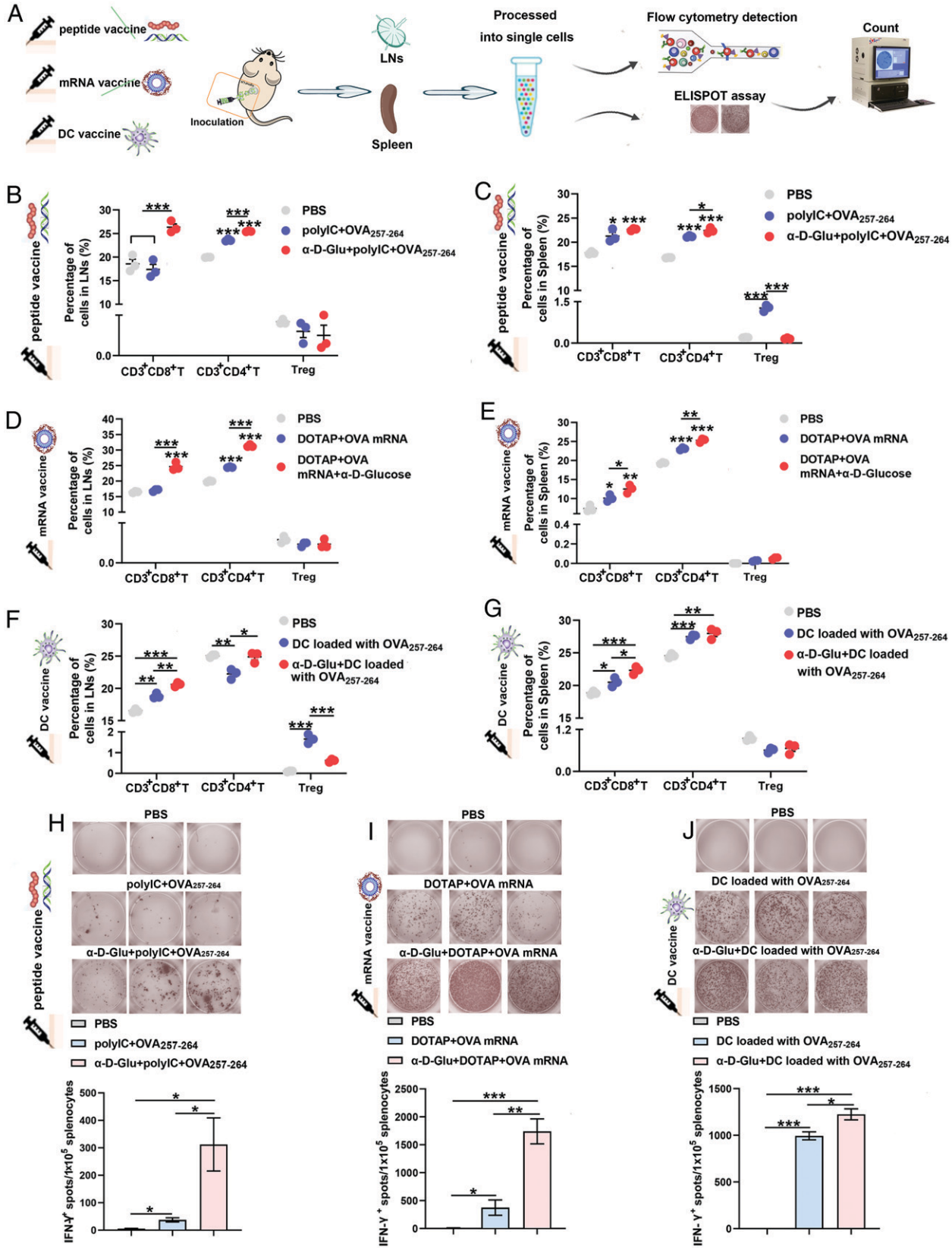

FIGURE 3. α-D-Glu enhanced the Ag-specific lymphocyte response to the neoantigen vaccine. (**A**) Schematic diagram of the experimental procedure. Detecting the effect of α-D-Glu+poly(I:C)+$OVA_{257–264}$ on T cell proportion in (**B**) the LNs and (**C**) spleen. Detecting the effect of α-D-Glu+DOTAP+OVA mRNA on T cell proportion in (**D**) the LNs and (**E**) spleen. Detecting the effect of α-D-Glu+poly(I:C)+$OVA_{257–264}$ on T cell proportion in the (**F**) LNs and (**G**) spleen. Collected splenic T cells analyzed by ELISPOT assays to detect Ag-specific T cells secreting IFN-γ in the (**H**) α-D-Glu+poly(I:C)+$OVA_{257–264}$ vaccine, (**I**) α-D-Glu+DOTAP+OVA mRNA vaccine, and (**J**) α-D-Glu combined with DC vaccine loaded with LPS+CPG+IFN-γ+$OVA_{257–264}$ vaccine groups. All data are representative of results from three independent experiments ($n = 3$). Significance was calculated using one-way ANOVA with multiple comparisons tests. $^*p < 0.05$, $^{**}p < 0.01$, $^{***}p < 0.001$.

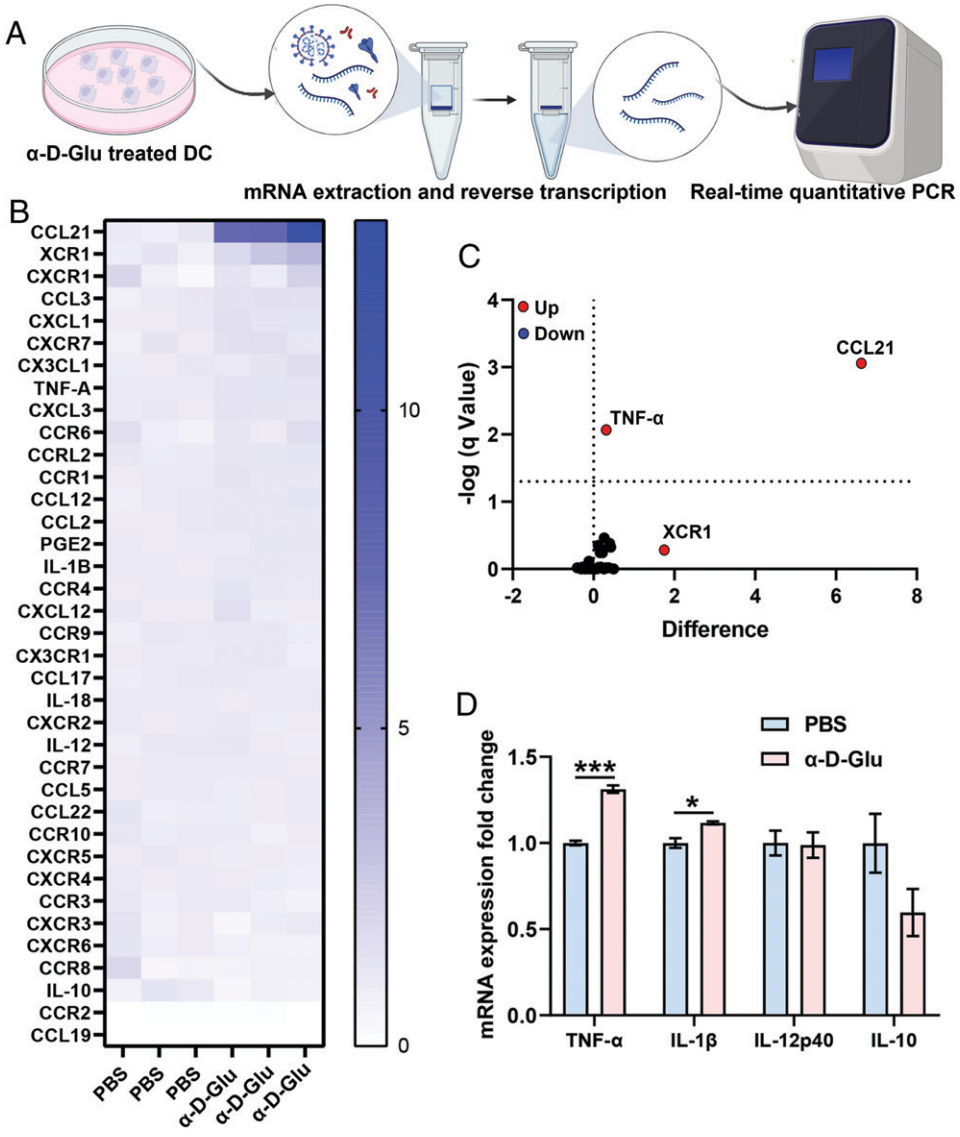

FIGURE 4. Analysis of chemokines and their receptors in α-D-Glu–treated DCs. (**A**) Schematic diagram of the experimental procedure. (**B**) Gene expression heatmap. (**C**) Gene expression dot plot. (**D**) Histogram of differentially expressed genes. All data are representative of results from three independent experiments ($n = 3$). Significance was calculated using one-way ANOVA with multiple comparisons tests. $^{*}p < 0.05$, $^{***}p < 0.001$.

companies, such as Pfizer and Novartis, have invested heavily in developing and expanding their immunotherapy product lines and actively acquiring related biologic companies to make further progress. Currently, >2000 immunotherapy programs have entered clinical trials worldwide (data are from http://clinicaltrials.gov), with research hotspots focusing on (1) adoptive immune cell therapy, mainly chimeric Ag receptor T cell therapy but also tumor-infiltrating lymphocyte therapy and engineered modified TCR therapies (19); (2) immune checkpoint inhibitor therapies (including mAbs and small-molecule inhibitors targeting PD-1/PD-L1, CTLA-4, and other reported immune checkpoint inhibitors) and their combination with other therapeutic modalities (including radiotherapy, chemotherapy, lytic virus therapy, etc.) (20); and (3) genomics- and bioinformatics-based screening for tumor mutations generating neoantigens (neoantigens) for individualized tumor vaccines, including peptide, mRNA, viral vector, and DC vaccines (21, 22). Although therapies that augment tumor-specific T cell responses with immune checkpoint inhibitor Abs or chimeric Ag receptor T cells have achieved new breakthroughs in tumor immunotherapy, there is still an urgent need for other immunotherapies and combination immunotherapies that actively stimulate endogenous antitumor T cells and generate long-term memory (23). Vaccination strategies are a direct approach to induce an effective immune response and long-term memory against cancer Ags and to actively stimulate endogenous antitumor T cells.

In most cases, vaccination against cancer Ags depends on DCs. DCs are the sentinels of the immune system; they initiate and direct the immune response. DCs can engulf, process, and present Ags to T cells and other immune cells, thereby initiating cancer-specific immune responses. In recent years, there has been extensive interest in how to further enhance the in vivo effects of new Ag-based vaccines. A large number of studies have focused on improving Ag selection and loading methods, DC preparation and culture methods, and vaccine delivery routes to enhance the efficacy of neoantigen vaccines (24, 25). We have also performed much research on related aspects previously, mainly focusing on (1) changing the method of Ag loading, (2) optimizing the culture method of DCs, (3) optimizing the conditions for stimulating DC maturation, and (4) optimizing the phenotype of prepared DCs to enhance the antitumor effect of DC vaccines (13, 26, 27). However, there is still a lack of relevant studies on enhancing the effectiveness of DC vaccines by improving the efficiency of DC migration to LNs. Migration from nonlymphoid to lymphoid tissues is a key feature of DCs. The ability of DCs to migrate is critical for triggering protective proinflammatory responses and tolerogenic immune responses. Understanding

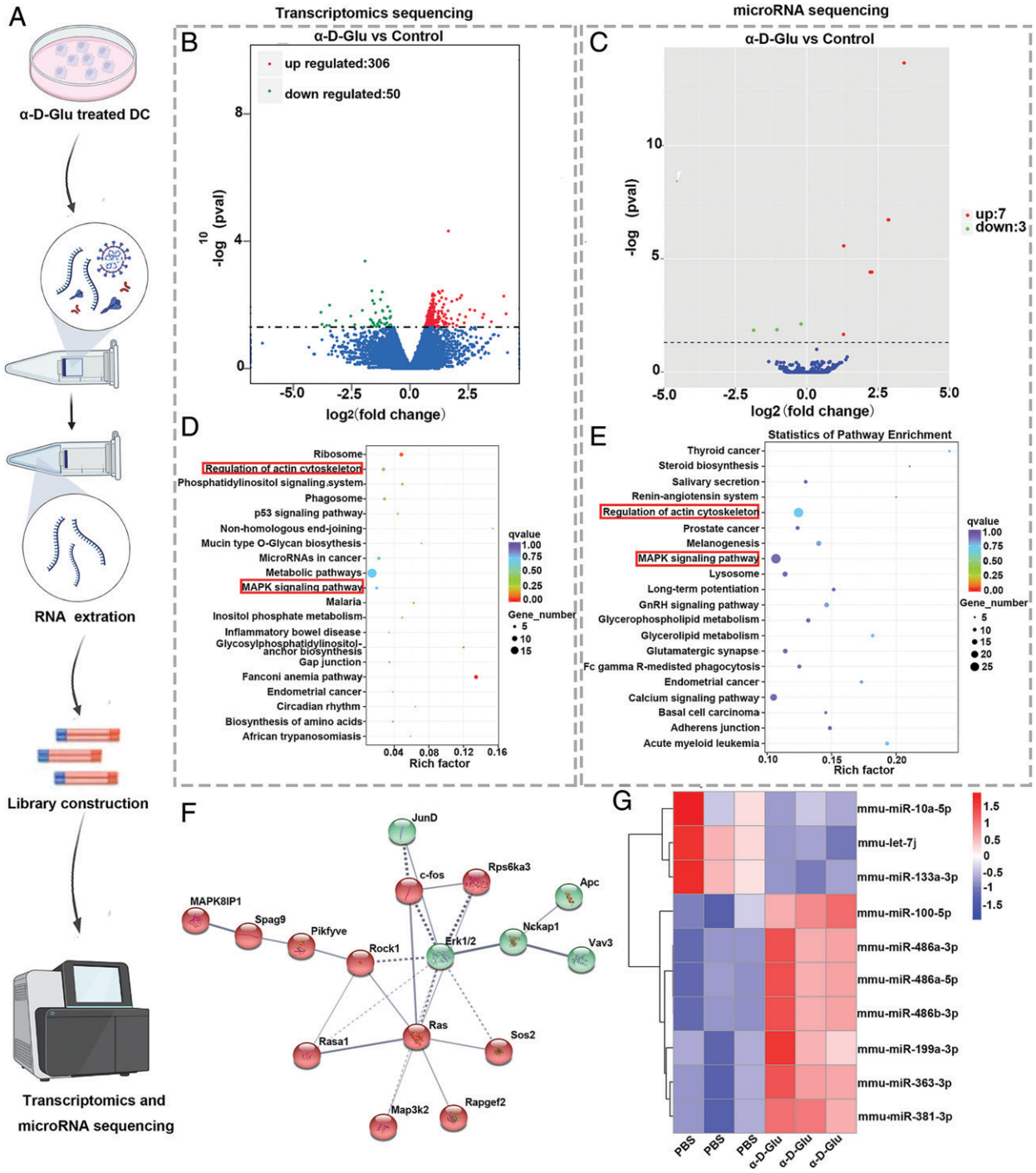

FIGURE 5. Transcriptomic and miRNA sequencing results after α-D-Glu treatment of DCs. (**A**) Schematic diagram of the experimental procedure. (**B**) Volcano plot of differentially expressed genes (DEGs) in DCs before and after α-D-Glu treatment. (**C**) Volcano plot of differentially expressed miRNAs in DCs before and after α-D-Glu treatment. (**D**) Kyoto Encyclopedia of Genes and Genomes (KEGG) pathway enrichment analysis of DEGs after α-D-Glu treatment. (**E**) KEGG pathway enrichment analysis of target genes of differentially expressed miRNAs after α-D-Glu treatment. (**F**) STRING analysis of actin cytoskeleton signaling pathway– and MAPK signaling pathway–related DEGs of DCs after α-D-Glu treatment. (**G**) Cluster analysis of differentially expressed miRNAs.

and controlling DC migration will support the development of new therapeutic and vaccination strategies.

Despite our increased understanding of the immunological roles and molecular mechanisms of DC migration during inflammation and immunity, several intriguing and important aspects of this field remain obscure and warrant further investigation. DCs have unique immunological functions, including Ag sensing, Ag capture, inflammatory cytokine production, chemotactic migration, and T cell stimulation and regulation. The overlap of the DC migration process with other aspects of DC function is critical for ensuring the most efficient and beneficial immune outcome, yet the understanding of the underlying mechanisms is limited. With the rapid development of single-cell technologies, single-molecule technologies, high-resolution in vivo imaging, and multiomics-based techniques, it will be possible to uncover the molecular activities and pathways that regulate DC migration and various inflammatory and immunological processes and develop new ideas for therapeutic strategies targeting DC migration in relevant immunological diseases. Recently, there has

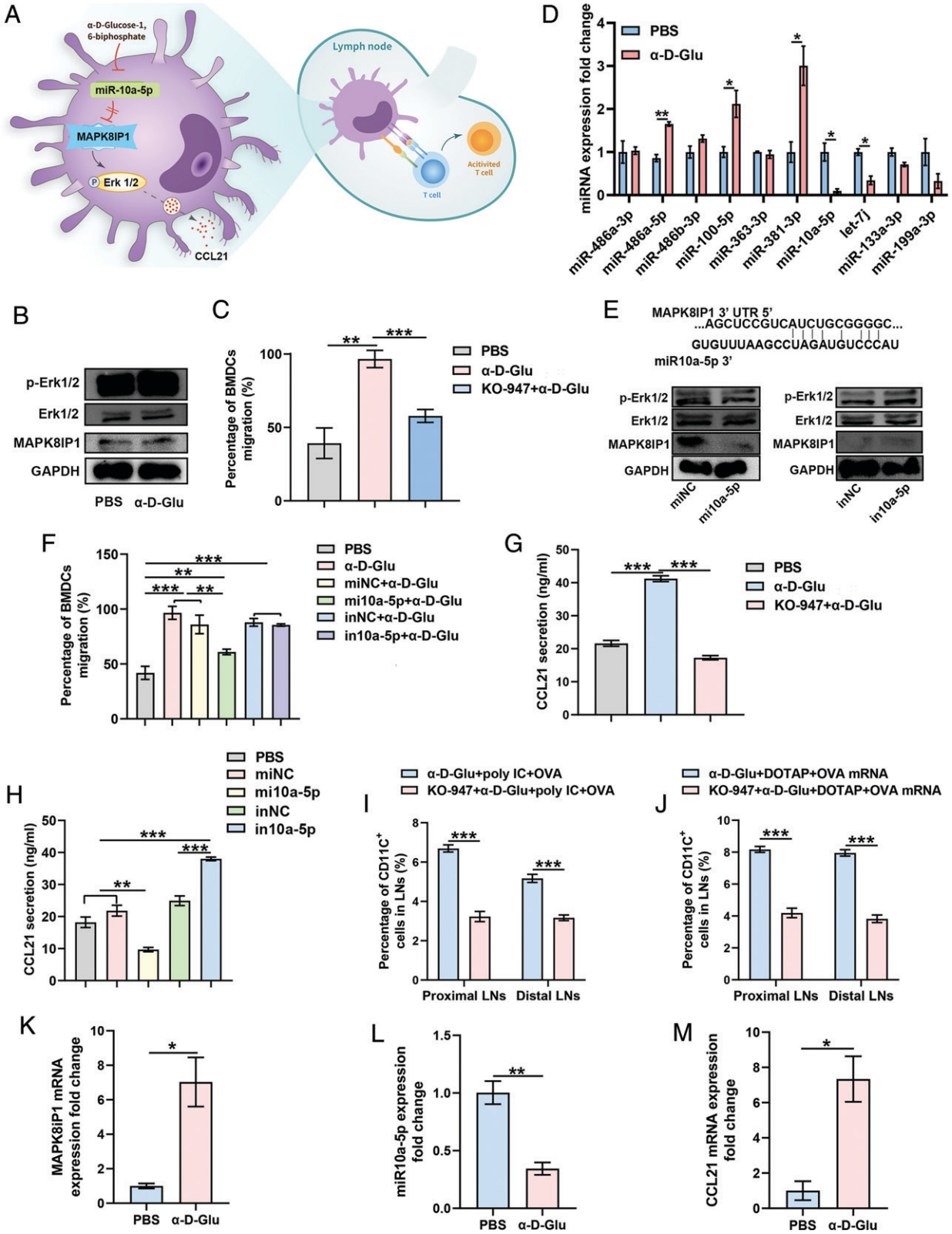

FIGURE 6. α-D-Glu promoted CCL21 secretion and induced DC migration by inhibiting miR-10a-5p and thereby activating the MAPK8IP1/ERK signaling pathway. (**A**) Diagram of the DC migration mechanism. (**B**) α-D-Glu activated the expression of MAPK8IP1 and p-ERK1/2 in DCs. (**C**) Inhibition of ERK in vitro inhibited α-D-Glu–mediated cell migration ($n = 3$). (**D**) miRNA expression was verified by RT-PCR ($n = 3$). (**E**) miR-10a-5p overexpression inhibited the expression of MAPK8IP1 and p-ERK1/2. (**F**) miR-10a-5p overexpression inhibited α-D-Glu–mediated cell migration ($n = 3$). (**G**) Inhibition of ERK in vitro inhibited α-D-Glu–mediated CCL21 secretion ($n = 3$). (**H**) miR-10a-5p overexpression inhibited CCL21 secretion ($n = 3$). (**I** and **J**) KO-947 inhibits α-D-Glu–induced DC migration in vivo ($n = 3$). (**K**) MAPK8IP1 expression in DCs in mouse LNs ($n = 5$). (**L**) CCL21 expression in DCs in mouse LNs ($n = 5$). (**M**) miR-10a-5p expression in DCs in mouse LNs ($n = 5$). Significance was calculated using one-way ANOVA with multiple comparisons tests. $^{*}p < 0.05$, $^{**}p < 0.01$, $^{***}p < 0.001$.

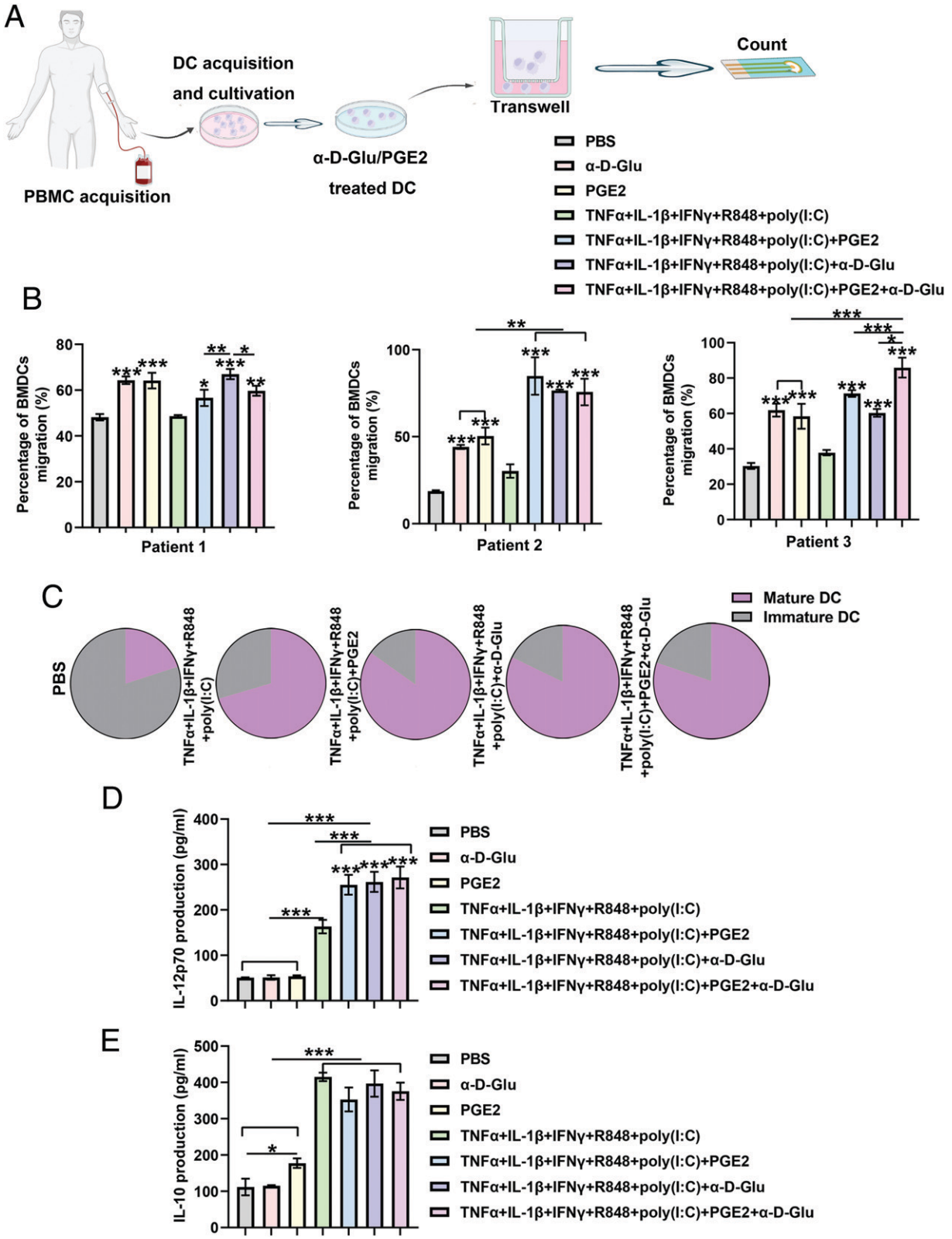

FIGURE 7. Preclinical efficacy evaluation of α-D-Glu. (**A**) Schematic diagram of the experimental procedure. (**B**) DC migration assay in patient-derived MoDCs ($n = 3$). (**C**) DC maturation assay in patient-derived MoDCs ($n = 3$). (**D** and **E**) The secretion of cytokines by MoDCs treated with different treatments was detected by ELISAs ($n = 3$). $^{*}p < 0.05$, $^{**}p < 0.01$, $^{***}p < 0.001$.

been a flurry of research on metabolites that support cancer immunotherapy, focusing on using intestinal flora-derived metabolites to enhance immunotherapy (28, 29), modulating the metabolism of immune cells themselves to enhance immunotherapy (30, 31), and altering tumor cell metabolism to enhance immunotherapy (32).

In this study, we mainly focused on the key scientific problem of low DC migration efficiency, which limits the efficacy of neoantigen-

based personalized immunotherapy. Using the selected metabolite α-D-Glu, which can improve the efficiency of DC migration in vitro and homing efficiency in vivo, we conducted an experiment to evaluate the antitumor effects of combination with a peptide Ag vaccine, mRNA vaccine encoding an Ag, and DC vaccine loaded with an Ag. We clarified the mechanism by which α-D-Glu regulates the expression of miR-10a-5p to promote DC migration through the MAPK signaling pathway. This provides an alternative strategy for further improving the efficacy of neoantigen-based immunotherapy in the future. Importantly, in the relevant tests of the patients' MoDCs, we found that the effect of α-D-Glu in inducing DC migration was equivalent to that of PGE_2, which promotes DC migration in the gold standard formula of clinical trials.

This study demonstrated that α-D-Glu can enhance the antitumor effects of vaccines by promoting DC homing. However, DC migration to tumor tissue has also been reported to enhance antitumor effects (33). Therefore, it is possible that the enhanced efficacy achieved with α-D-Glu combined with neoantigen-based immunotherapy may also be achieved by the combination of promoting LN homing by DCs and DC migration to tumor tissues. An attempt was made to investigate DC migration to tumor tissue, but these events could not be demonstrated at this time because the number of DCs in the tumor fraction is too small, and it is difficult to quantify DCs in tumor tissue after fluorescence labeling. In future studies, we will optimize the intratumoral quantification and tracing of DCs to further elucidate whether the enhanced efficacy of α-D-Glu in neoantigen-based immunotherapy is related to DC migration to tumor tissue.

Overall, α-D-Glu increases DC migration, leading to improved efficacy of neoantigen (peptide, mRNA) vaccines and Ag-loaded DC vaccines used in combination with α-D-Glu. Thus, this strategy can be relatively easily translated into clinical protocols being used to treat cancer with neoantigen-based immunotherapies.

Disclosures

The authors have no financial conflicts of interest.

References

1. Ott, P. A., Z. Hu, D. B. Keskin, S. A. Shukla, J. Sun, D. J. Bozym, W. Zhang, A. Luoma, A. Giobbie-Hurder, L. Peter, et al. 2017. An immunogenic personal neoantigen vaccine for patients with melanoma. [Published erratum appears in 2018 Nature 555: 402.] *Nature* 547: 217–221.
2. Sahin, U., E. Derhovanessian, M. Miller, B. P. Kloke, P. Simon, M. Löwer, V. Bukur, A. D. Tadmor, U. Luxemburger, B. Schrörs, et al. 2017. Personalized RNA mutanome vaccines mobilize poly-specific therapeutic immunity against cancer. *Nature* 547: 222–226.
3. Hilf, N., S. Kuttruff-Coqui, K. Frenzel, V. Bukur, S. Stevanovic, C. Gouttefangeas, M. Platten, G. Tabatabai, V. Dutoit, S. H. van der Burg, et al. 2019. Actively personalized vaccination trial for newly diagnosed glioblastoma. [Published erratum appears in 2019 Nature 566: E13.] *Nature* 565: 240–245.
4. Keskin, D. B., A. J. Anandappa, J. Sun, I. Tirosh, N. D. Mathewson, S. Li, G. Oliveira, A. Giobbie-Hurder, K. Felt, E. Gjini, et al. 2019. Neoantigen vaccine generates intratumoral T cell responses in phase Ib glioblastoma trial. *Nature* 565: 234–239.
5. Zhao, J. F., A. X. Chen, R. D. Gartrell, A. M. Silverman, L. Aparicio, T. Chu, D. Bordbar, D. Shan, J. Samanamud, A. Mahajan, et al. 2019. Immune and genomic correlates of response to anti-PD-1 immunotherapy in glioblastoma. [Published erratum appears in 2019 Nat. Med 25: 1022.] *Nat. Med.* 25: 462–469.
6. Ott, P. A., S. Hu-Lieskovan, B. Chmielowski, R. Govindan, A. Naing, N. Bhardwaj, K. Margolin, M. M. Awad, M. D. Hellmann, J. J. Lin, et al. 2020. A phase Ib trial of personalized neoantigen therapy plus anti-PD-1 in patients with advanced melanoma, non-small cell lung cancer, or bladder cancer. *Cell* 183: 347–362.e24.
7. Seyfizadeh, N., R. Muthuswamy, D. A. Mitchell, S. Nierkens, and N. Seyfizadeh. 2016. Migration of dendritic cells to the lymph nodes and its enhancement to drive anti-tumor responses. *Crit. Rev. Oncol. Hematol.* 107: 100–110.
8. Mitchell, D. A., K. A. Batich, M. D. Gunn, M. N. Huang, L. Sanchez-Perez, S. K. Nair, K. L. Congdon, E. A. Reap, G. E. Archer, A. Desjardins, et al. 2015. Tetanus toxoid and CCL3 improve dendritic cell vaccines in mice and glioblastoma patients. *Nature* 519: 366–369.
9. Zhang, R., L. Tang, Q. Li, Y. Tian, B. Zhao, B. Zhou, and L. Yang. 2021. Cholesterol modified DP7 and pantothenic acid induce dendritic cell homing to enhance the efficacy of dendritic cell vaccines. *Mol. Biomed.* 2: 37.
10. Ding, Z., Q. Li, R. Zhang, L. Xie, Y. Shu, S. Gao, P. Wang, X. Su, Y. Qin, Y. Wang, et al. 2021. Personalized neoantigen pulsed dendritic cell vaccine for advanced lung cancer. *Signal Transduct. Target. Ther.* 6: 26.
11. Gross, S., M. Erdmann, I. Haendle, S. Voland, T. Berger, E. Schultz, E. Strasser, P. Dankerl, R. Janka, S. Schliep, et al. 2017. Twelve-year survival and immune correlates in dendritic cell-vaccinated melanoma patients. *JCI Insight* 2: e91438.
12. Kuai, R., L. J. Ochyl, K. S. Bahjat, A. Schwendeman, and J. J. Moon. 2017. Designer vaccine nanodiscs for personalized cancer immunotherapy. *Nat. Mater.* 16: 489–496.
13. Zhang, R., L. Tang, Y. Tian, X. Ji, Q. Hu, B. Zhou, D. Zhenyu, X. Heng, and L. Yang. 2020. Cholesterol-modified DP7 enhances the effect of individualized cancer immunotherapy based on neoantigens. *Biomaterials* 241: 119852.
14. Burrows, F., L. Kessler, J. Chen, X. Gao, R. Hansen, S. Li, C. Thach, L. Darjania, Y. Yao, Y. Wang, et al. 2017. Abstract 5168: KO-947, a potent ERK inhibitor with robust preclinical single agent activity in MAPK pathway dysregulated tumors. *Cancer Res.* 77 (Suppl. 13): 5168.
15. Chiang, C. L., L. E. Kandalaft, J. Tanyi, A. R. Hagemann, G. T. Motz, N. Svoronos, K. Montone, G. M. Mantia-Smaldone, L. Smith, H. L. Nisenbaum, et al. 2013. A dendritic cell vaccine pulsed with autologous hypochlorous acid-oxidized ovarian cancer lysate primes effective broad antitumor immunity: from bench to bedside. *Clin. Cancer Res.* 19: 4801–4815.
16. Kong, W., L. Yang, P. P. Li, Q. Q. Kong, H. Y. Wang, G. X. Han, and Q. B. Wang. 2018. MiR-381-3p inhibits proliferation, migration and invasion by targeting LRP6 in papillary thyroid carcinoma. *Eur. Rev. Med. Pharmacol. Sci.* 22: 3804–3811.
17. Lu, Y., G. Wei, L. Liu, Y. Mo, Q. Chen, L. Xu, R. Liao, D. Zeng, and K. Zhang. 2017. Direct targeting of MAPK8IP1 by miR-10a-5p is a major mechanism for gastric cancer metastasis. *Oncol. Lett.* 13: 1131–1136.
18. Miyagaki, T., M. Sugaya, H. Okochi, Y. Asano, Y. Tada, T. Kadono, A. Blauvelt, K. Tamaki, and S. Sato. 2011. Blocking MAPK signaling downregulates CCL21 in lymphatic endothelial cells and impairs contact hypersensitivity responses. *J. Invest. Dermatol.* 131: 1927–1935.
19. June, C. H., R. S. O'Connor, O. U. Kawalekar, S. Ghassemi, and M. C. Milone. 2018. CAR T cell immunotherapy for human cancer. *Science* 359: 1361–1365.
20. Ribas, A., and J. D. Wolchok. 2018. Cancer immunotherapy using checkpoint blockade. *Science* 359: 1350–1355.
21. Sahin, U., and Ö. Türeci. 2018. Personalized vaccines for cancer immunotherapy. *Science* 359: 1355–1360.
22. Hu, Z., P. A. Ott, and C. J. Wu. 2018. Towards personalized, tumour-specific, therapeutic vaccines for cancer. *Nat. Rev. Immunol.* 18: 168–182.
23. Harari, A., M. Graciotti, M. Bassani-Sternberg, and L. E. Kandalaft. 2020. Antitumour dendritic cell vaccination in a priming and boosting approach. *Nat. Rev. Drug Discov.* 19: 635–652.
24. van Gulijk, M., F. Dammeijer, J. G. J. V. Aerts, and H. Vroman. 2018. Combination strategies to optimize efficacy of dendritic cell-based immunotherapy. *Front. Immunol.* 9: 2759.
25. Mehta, N. K., K. D. Moynihan, and D. J. Irvine. 2015. Engineering New Approaches to Cancer Vaccines. *Cancer Immunol. Res.* 3: 836–843.
26. Zhang, R., F. Yuan, Y. Shu, Y. Tian, B. Zhou, L. Yi, X. Zhang, Z. Ding, H. Xu, and L. Yang. 2020. Personalized neoantigen-pulsed dendritic cell vaccines show superior immunogenicity to neoantigen-adjuvant vaccines in mouse tumor models. *Cancer Immunol. Immunother.* 69: 135–145.
27. Zhang, R., L. Tang, Y. Tian, X. Ji, Q. Hu, B. Zhou, Z. Ding, H. Xu, and L. Yang. 2020. DP7-C-modified liposomes enhance immune responses and the antitumor effect of a neoantigen-based mRNA vaccine. *J. Control. Release* 328: 210–221.
28. Luu, M., Z. Riester, A. Baldrich, N. Reichardt, S. Yuille, A. Busetti, M. Klein, A. Wempe, H. Leister, H. Raifer, et al. 2021. Microbial short-chain fatty acids modulate $CD8^+$ T cell responses and improve adoptive immunotherapy for cancer. *Nat. Commun.* 12: 4077.
29. Mager, L. F., R. Burkhard, N. Pett, N. C. A. Cooke, K. Brown, H. Ramay, S. Paik, J. Stagg, R. A. Groves, M. Gallo, et al. 2020. Microbiome-derived inosine modulates response to checkpoint inhibitor immunotherapy. *Science* 369: 1481–1489.
30. Li, X., M. Wenes, P. Romero, S. C. C. Huang, S. M. Fendt, and P. C. Ho. 2019. Navigating metabolic pathways to enhance antitumour immunity and immunotherapy. *Nat. Rev. Clin. Oncol.* 16: 425–441.
31. Yang, W., Y. Bai, Y. Xiong, J. Zhang, S. Chen, X. Zheng, X. Meng, L. Li, J. Wang, C. Xu, et al. 2016. Potentiating the antitumour response of CD8(+) T cells by modulating cholesterol metabolism. *Nature* 531: 651–655.
32. Zhang, Y., R. Kurupati, L. Liu, X. Y. Zhou, G. Zhang, A. Hudaihed, F. Filisio, W. Giles-Davis, X. Xu, G. C. Karakousis, et al. 2017. Enhancing $CD8^+$ T cell fatty acid catabolism within a metabolically challenging tumor microenvironment increases the efficacy of melanoma immunotherapy. *Cancer Cell* 32: 377–391.e9.
33. Zhang, R., L. Tang, B. Zhao, Y. Tian, B. Zhou, Y. Mu, and L. Yang. 2021. A peptide-based small RNA delivery system to suppress tumor growth by remodeling the tumor microenvironment. *Mol. Pharm.* 18: 1431–1443.